



**High resolution monitoring, real time visualization
and reliable modeling of highly controlled,
intermediate and up-scalable size pilot injection
tests of underground storage of CO₂**

Contract #309067

Deliverable Number D4.3
Title Modeling and interpretation of the results of the injection experiments (Part1)
Work-Package 4

Lead Participant UU
Contributors Saba Joodaki, Zhibing Yang, Maryeh Hedayati and Auli Niemi (UU)
Jacob Bensabat (EWRE)

Date: 28.5.2018

Dissemination level PU

Executive summary

This Deliverable presents the first model interpretations of Heletz, Israel residual trapping experiments, the **Residual Trapping Experiment I (RTE I)** carried out in September 2016 and the **Residual Trapping Experiment II (RTE II)** carried out in August to November 2017. The actual experiments and the experimental results are described in TRUST Deliverables 2.3-2.4 – Part I. The residual trapping experiments are based on the principle of a combination of hydraulic, thermal and/or tracer tests before and after creating the residually trapped zone of CO₂ and using the difference in the responses of these tests to estimate the in-situ residual trapping. The first experiment, RTE I, is based on hydraulic withdrawal tests before and after the creation of the residually trapped zone. In this experiment, the residually trapped zone was also created by fluid withdrawal, by first injecting CO₂, then withdrawing fluids until CO₂ was at residual saturation. In the second test, RTE II, the main characterization method was injection/withdrawal of water and partitioning tracers, whose recovery with and without residually trapped CO₂ in the formation was compared. In this second experiment the residually trapped zone was created by first injecting CO₂ and then injecting water saturated with CO₂ to push away the mobile CO₂ and leaving the residually trapped zone behind.

Here, the experimental results of **RTE I** have been modelled first. A simplified analytical model was first used for guidance, followed by 'full-physics' modeling with the TOUGH2 simulator, where all the data (temperature, pressure, flow rates, two-phase flow behavior etc.) were matched. Comprehensive calibration procedure led to a best-estimate of the test behavior, suggesting an in-situ residual saturation of 0.1, including a hysteretic behavior in the relative permeability functions, similar properties in the two reservoir layers and preference of the CO₂ to enter the upper layer.

The 'full-physics' model calibrated with RTE I was then used to model the later **RTE II**. Without any further calibration, the results showed a perfect agreement for the early parts of the experiment (prior to establishing the residually trapped zone) and relatively good agreement even with the later parts, with residually trapped CO₂ in the formation. In particular, the amount of the tracer partitioned into CO₂ was well captured with the earlier calibrated model, without any further adjustments, indicating a similar estimate of residually trapped CO₂ than from RTE I. Due to time considerations - in terms of the data from RTE II becoming available for modeling - the modeling of RTE II is still in progress at the time of final reporting of TRUST project and writing of this deliverable. As of the results so far it seems, however, that the conclusions from RTE I give a good estimation of the residual trapping at Heletz.

The second part of the test interpretation (Deliverable 4.6 'Modeling and interpretation of the results of the injection experiments (Part2)') presents additional modeling of these residual trapping experiments, especially RTE I. In particular, it will present (i) a detailed modeling of the coupled well-reservoir behavior during the experiment, thereby giving information concerning the CO₂ lost during the self-release period and (ii) an in-depth analysis of the hydraulic response of the characterization tests, in terms of what information a hydraulic test can provide about the system being tested.

Altogether, the modeling carried out in Deliverables 4.3 and 4.6 will provide a good understanding of the system performance during CO₂ injection and the resulting residual trapping. The analysis work and summarizing the results will continue beyond the time of final reporting for TRUST and the resulting peer-reviewed publications will be uploaded to the TRUST web-site.

Keywords	CO ₂ injection, residual trapping, Heletz pilot injection site
----------	---

Table of Contents

1. Introduction	4
2. Model for the site	4
2.1 Overview.....	4
2.2 Two-phase flow properties	5
2.3 Modeling approaches	8
3. Modeling of the Residual Trapping Experiment I (RTE I)	8
3.1 Test sequence and first estimates.....	8
3.2 Modelling the test sequence with full two-phase model (TOUGH2).....	9
3.2.1 Cases considered	9
3.2.2 Assuming equal permeability in the two reservoir layers.....	11
3.2.2 Assuming different properties in the two reservoir layers.....	12
3.2.3 Accounting for relative permeability hysteresis.....	15
3.2.4 Modelling the temperature response	15
3.2.5 Modified conceptual model	17
3.3 Conclusions.....	20
4. Modeling of the Residual Trapping Experiment II.....	20
4.1 Test sequence	20
4.2 Modeling the first phases of the experiment.....	21
4.3 Modelling phases after the CO2 saturated water injection	24
4.3.1 The effect of relative permeability function.....	24
4.3.2 Hysteretic model	27
4.4 Conclusions.....	30
5. Conclusions	31
6. References	32
Appendix A	Error! Bookmark not defined.
Table 1.....	Error! Bookmark not defined.
Parameter used for pressure analysis.....	Error! Bookmark not defined.

1. Introduction

Residual trapping is a critical site-specific parameter for any CO₂ injection project. However, estimating this parameter in scales larger than laboratory scales is challenging. In fact, one of the very few experiments performed to estimate the parameter of residual gas saturation in the field scale, is the CO₂CRC project at Otway, Australia (Paterson et al., 2014, Dance & Paterson 2016) 2016). As a result, finding appropriate approaches to quantify this parameter in field scales is important in order to estimate the durability and safety of a storage. At Heletz, Israel, two fundamentally different field scale experiments for quantifying residual trapping have been carried out, the Residual Trapping Experiment I in the autumn of 2016 and the Residual Trapping Experiment II in the autumn of 2017.

The actual experiments and the experimental results are described in TRUST Deliverable 2.3-2.4 – Part 1. The residual trapping experiments are based on the principle of a combination of hydraulic, thermal and/or tracer tests before and after creating the residually trapped zone of CO₂ and using the difference in the responses of these tests to estimate the in-situ residual trapping. The first experiment, RTE I, is based on hydraulic withdrawal tests before and after the creation of the residually trapped zone. In this experiment, the residually trapped zone was also created by fluid withdrawal, by first injecting CO₂, then withdrawing fluids until CO₂ was at residual saturation. In the second test, RTE II, the main characterization method was injection/withdrawal of water and partitioning tracers, whose recovery with and without residually trapped CO₂ in the formation was compared. In this second experiment the residually trapped zone was created by first injecting CO₂ and then injecting water saturated with CO₂ to push away the mobile CO₂ and leaving the residually trapped zone behind.

In this report these two experiments are modelled and analyzed in terms of in-situ residual trapping. Due to time issues, the results for RTE I can be already considered mature and conclusive, while the results for RTE II are still somewhat preliminary and presenting results for work in progress.

2. Model for the site

2.1 Overview

The conceptual model used for interpreting the test results is based on the extensive site characterization studies at the Heletz site (see e.g. Niemi et al. 2016) as well as the large number of predictive modeling studies carried out for the purpose of experiment planning (e.g. Rasmusson et al. 2014). Due to the extensive pre-investigations, a good understanding exists concerning the location of the reservoir and cap-rock layers and all their key properties, such as permeability, porosity, two-phase flow properties and other

relevant site properties. For details concerning these site properties the reader is referred to e.g. Niemi et al. (2016). This previous information was used when building up the models for interpreting the RTE I and RTE II.

For modeling of the experiments, the conceptual model used includes the two sandstone layers A and W, exposed to CO₂ injection. These have thicknesses of 2m and 9m, respectively, and are separated by a 3m thick shale layer. A schematic conceptual model is shown in Figure 1. The horizontal length of the model is 500m and the outer edge boundary, which is far away from the point of injection, is defined as a specified pressure condition. No-flow boundary was assumed for the top and the bottom of the model representing the impermeable formations that bound the aquifer from above and below. Different permeability values that were deemed reasonable in the light of various core and in-situ permeability measurements were used and varied in the calibration process. Overview of the parameter values used in the modeling is shown in Table 1.

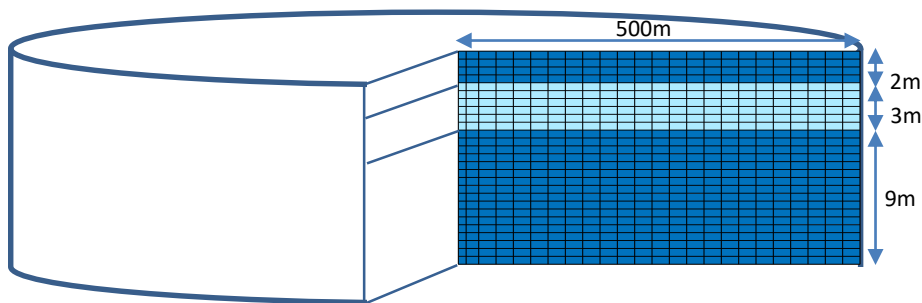


Figure 1. A schematic figure of the applied radial symmetric model

2.2 Two-phase flow properties

Given that the residual trapping is the key parameter to be identified from the study, the two-phase flow characteristic functions deserve special attention. Measurements of relative permeability (Figure 2.) and capillary pressure functions have been carried out on Heletz cores (Benson et al. 2015; Hingerl et al. 2016). This data was used as basis for modelling the hysteretic and non-hysteretic relative permeabilities and capillary pressures.

Table 1. Summary of parameter values used in the simulation, values that were varies in calibration are given in Table 2.

Symbol	Parameter	Value
Brooks-Corey parameters, non-hysteretic model		
S_{lr}	Residual liquid saturation	0.2
S_{gr}	Residual gas saturation	0.05, 0.07, 0.1, 0.2
Λ	Brooks-Corey fitting parameter	0.46
$P_0^{(*)}$	Entry pressure (Pa)	2850
Capillary pressure function, hysteretic model		
m^d	m for drainage in equation 8	0.3
S_{lmin}	Residual liquid saturation for P_c	0.03
$P_0^{d(*)}$	Capillary strength parameter (drainage) (Pa)	2.68×10^3
m^w	m for imbibition in equation 8	0.3
P_0^w	Capillary strength parameter (imbibition) (Pa)	2.68×10^3
Relative permeability function, hysteretic model		
M	Van Genuchten m for k_{rl} (eq.6)	0.6
S_{lr}	Residual liquid saturation	0.3
S_{grmax}	Maximum residual gas saturation	0.1, 0.2
k_{rgmax}	Maximum k_{rg}	0.7
M	Van Genuchten m for k_{rg} (eq. 3)	0.8
Formation properties		
P	Bottom-hole Pressure (Pa)	1.45×10^7
T	Initial temperature (°C)	64
	Salinity (mg liter ⁻¹)	52502
Φ	Porosity	0.25
λ_{dry}	Dry heat conductivity (W m ⁻¹ °C ⁻¹)	1.8
λ_{wet}	Wet heat conductivity (W m ⁻¹ °C ⁻¹)	4.2

(*calibrated according to Leverett scaling based on permeability used, Table 2.

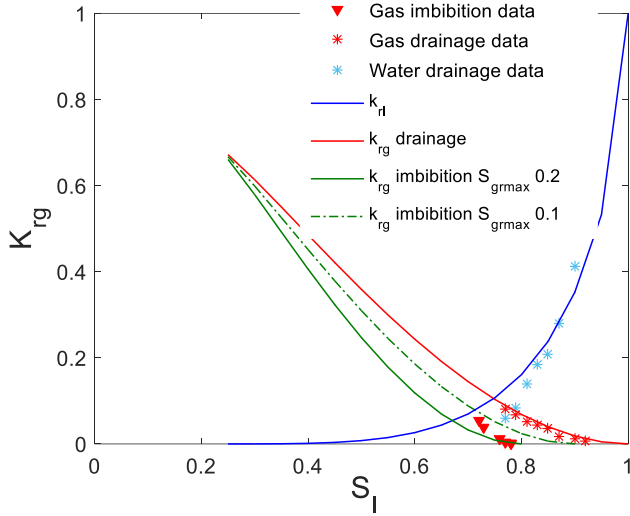


Figure 2. Relative permeability of gas and liquid measured by Benson et al., (2014) and fitted models.

Brooks-Corey model, as implemented in TOUGH simulator was used to model the relative permeability. Hysteresis effect on capillary pressure (P_c), liquid relative permeability (k_{rl}) and gas relative permeability (k_{rg}) curves were also investigated by applying the hysteresis model modified by Doughty (Equations 1-6) (Doughty 2013). The model defines the correlation between the gas residual trapping at the end of imbibition (S_{gr}^Δ) and gas saturation at the transition point (S_l^Δ), based on Land trapping model (Equation 1). The parameters used for the relative permeability functions were obtained by manual matching to the data presented in Hingerl et al. (2016). These parameters are summarized in Table 1.

$$S_{gr}^\Delta = \frac{1 - S_l^\Delta}{1 + \left[\frac{1}{S_{grmax}} - \frac{1}{(1 - S_{lr})} \right] (1 - S_l^\Delta)} \quad (1)$$

$$k_{rl} = \sqrt{\bar{S}_l} \left[1 - \left(1 - \frac{\bar{S}_{gt}}{1 - \bar{S}_l^\Delta} \right) \left(1 - (\bar{S}_l + \bar{S}_{gt})^{\frac{1}{m}} \right) - \left(\frac{\bar{S}_{gt}}{1 - \bar{S}_l^\Delta} \right) \left(1 - (\bar{S}_l^\Delta)^{\frac{1}{m}} \right) \right]^2 \quad (2)$$

$$k_{rg} = (1 - (\bar{S}_l + \bar{S}_{gt}))^\gamma (1 - (\bar{S}_l + \bar{S}_{gt})^{1/m})^{2m} \quad (3)$$

$$P_c = -P_0^\gamma \left[\left(\frac{S_l - S_{lmin}}{1 - S_{gr}^\Delta - S_{lmin}} \right)^{-\left(\frac{1}{m\gamma}\right)} - 1 \right]^{(1-m\gamma)} \quad (4)$$

where,

$$\bar{S}_{gt} = \frac{S_{gr}^\Delta (S_l - S_l^\Delta)}{(1 - S_{lr})(1 - S_l^\Delta - S_{gr}^\Delta)} \quad (5)$$

$$\bar{S}_l = \frac{S_l - S_{lr}}{1 - S_{lr}}, \quad \bar{S}_l^\Delta = \frac{S_l^\Delta - S_{lr}}{1 - S_{lr}} \quad (6)$$

2.3 Modeling approaches

The first estimation of the results of RTE I was made based on simple analytical solution by Theis (Appendix A). Then, full-physics TOUGH2 (Pruess et al. 1999) simulations were carried out to match the entire test sequences for both experiments. The equation-of-state (EOS) module ECO2N (Pruess 2005) was used to modelling the RTE I. For RTE II that also includes a partitioning tracer test, the EOS module EOS7C (Oldenburg et al. 2004) was applied.

The establishment of residual state by withdrawing the injected gas was simulated using the well deliverability option provided in TOUGH2. This option relates the mass production of the phase β to a specified bottom-hole pressure using a productivity index.

3. Modeling of the Residual Trapping Experiment I (RTE I)

3.1 Test sequence and first estimates

The test sequence of RTE I shown in Figure 3. Extensive presentation of the data is given in Deliverable 2.3 – 2.4 (Part 1) and will not be repeated here. The key data used for model calibration included the down-hole pressure and temperature measurements, measured fluid flow rates and U-tube fluid samples.

First estimates of the test behavior were made by using a simple analytical model for the analysis of the hydraulic withdrawal tests prior and after creating the residually trapped zone. These tests were carried out on September 9th and September 29th (Figure 3.). This analysis is presented in Appendix A and indicated essentially very small quantities of CO₂ being present in the formation at the time of the second experiment. This rough preliminary estimation thereby indicated relatively low residual trapping of CO₂.

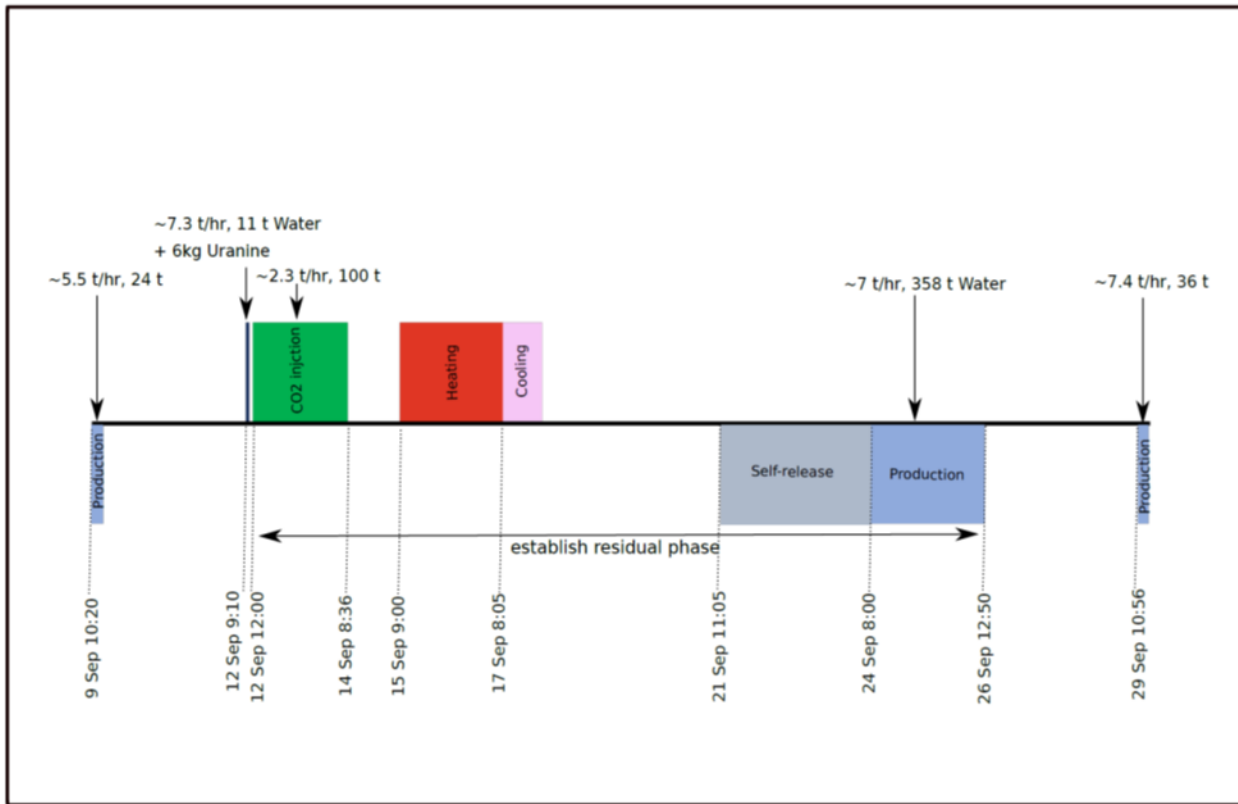


Figure 3. Test sequence of Residual Trapping Experiment I

3.2 Modelling the test sequence with full two-phase model (TOUGH2)

3.2.1 Cases considered

As the basis of pressure calibration the pressure data recorded at the lower sensor, PT76 was used. This sensor is located about 1m below the intermediate shale layer. The first hydraulic test (implemented on 9th of September) was used for first calibration of the model, to determine possible combinations the formation permeability. Based on this (and previous knowledge from in-situ hydraulic testing and permeability testing on cores), the possible combinations of meaningful permeabilities of the two reservoir layers A and W were determined and used in further analyses. The resulting permeability combinations are shown in Table 2, forming also the base of the further calibration cases. In further simulations different combinations of layer

permeabilities were used along with the assumed residual gas saturations and formation anisotropy, as well as taking into account for hysteresis in the two-phase characteristic functions (Table 2.)

Processes that take place in the well during gas injection (12th-14th September) and after well opening (21th-24th September) are highly complex and are addressed in more detail in Deliverable 4.6, with a coupled well-reservoir model. Here, to simulate the pressure fluctuation during the self-release period (21st and 24th of September) when the well was first opened, a somewhat simplified approach was used. The period was simulated in a number of steps by periodically assigning the measured bottom-hole pressure in the well as a boundary condition (to simulate the fluid flow from the formation towards the well) followed by a rest period (to simulate the release from the well). To model the fluid production using well deliverability, bottom-hole pressure was chosen based on the pressure data recorded in the sensor and corresponding flow rates were calculated by the model for both phases.

Table 2. Scenarios used in the calibration

Scenario	Permeability sand A (9m)	Permeability sand W (2m)	S _{gr} sand A	S _{gr} sand W	Anisotropy ratio*
Equal permeability in the layers					
1	400	400	0.2	0.2	3
2	400	400	0.1	0.1	3
3	400	400	0.07	0.07	3
4	400	400	0.05	0.05	3
Different permeability in the two layers					
5	300	750	0.1	0.1	1
6	300	750	0.05	0.05	1
7	300	750	0.05	0.1	1
8	300	750	0.1	0.05	1
9	400	400	0.1	0.1	1
Varying the residual saturation between the two layers					
10	400	400	0.1	0.05	3
11	400	400	0.05	0.1	3
12	100	1500	0.1	0.1	1
13**	400	400	0.2	0.2	3
14**	400	400	0.1	0.1	3
15**	400	400	0.05	0.05	3
16**	300	750	0.1	0.1	1
Hysteretic relative permeability model					
17	400	400	S _{grmax} 0.1	S _{grmax} 0.1	3
18	400	400	S _{grmax} 0.2	S _{grmax} 0.2	3
19**	400	400	S _{grmax} 0.1	S _{grmax} 0.1	3
20**	400	400	S _{grmax} 0.2	S _{grmax} 0.2	3

*) In case of same permeability in the two layers, anisotropy within the layer was used, in case of different layer permeabilities there was no anisotropy within a layer

**) Conceptual model 2 (Ch 3.2.5)

3.2.2. Assuming equal permeability in the two reservoir layers

It was shown that with the measured withdrawal rate of 5.5 ton/hr a homogeneous model with permeability of 400 mD would match the pressure drop from the first hydraulic test. Different meaningful combinations of residual saturation were tested with permeability of 400 mD in the two layers (uppermost cases in Table 2). Figure 4. Shows a comparison of simulated pressure for different residual gas saturations, along with the measured values at sensor PT76. For the sake of visual clarity of the figure, the self-release simulation results are not shown. Inspection of the results shows that the lowest residual saturations show the best agreement with the measured data.

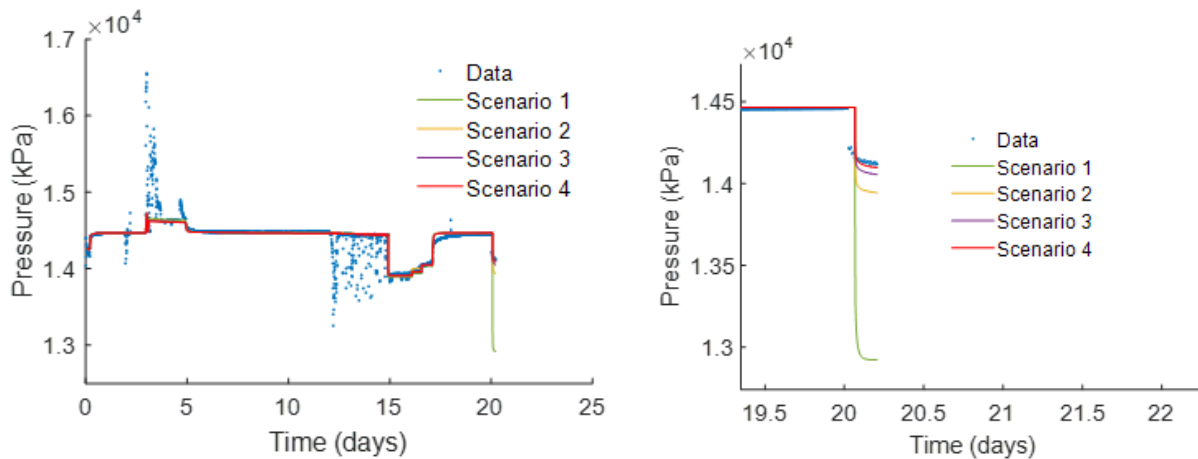


Figure 4. Pressure data and pressure simulation results of homogeneous models (Cases 1-4) with residual gas saturation of 0.2, 0.1, 0.07 and 0.05. Left panel shows the entire sequence and right panel shows a zoom-in to the last hydraulic test. (start of the experiment of 9th of September is time zero).

Calculated and measured liquid flow rates with these models are compared in Figure 5. It can be seen that the highest calculated flow rate is related to the case with the lowest residual saturation. It can also be noted that the measured flow data is more scattered in comparison with the calculated flow rates. Although simulation results of the calculated flow rates for all these different gas residual saturations fall within in the order of magnitude of the measured data, the case with gas residual saturation of 0.1, falling in the middle of the measured values, can be deemed to be in best agreement with the data. One test was done (not shown here) to back calculate the pressure assigning the flow rate. The results were in agreement with Figure 5, i.e. for the given average flow rate of 7 m³/hr, the simulation with residual gas saturation of 0.1 showed the best match with the pressure data.

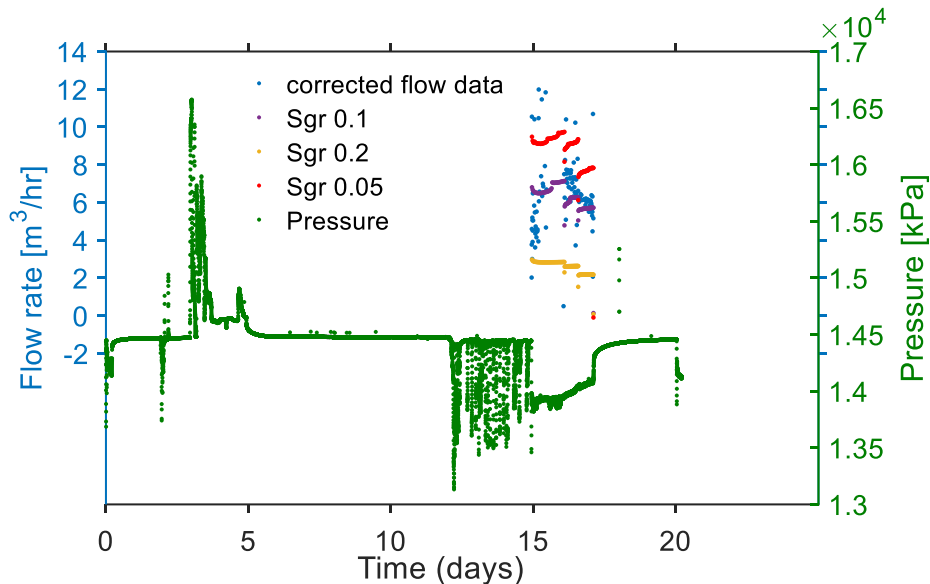


Figure 5. Measured and simulated flow rates during production phase (Cases 1,2, and 4, with residual gas saturation of 0.2, 0.1 and 0.05) (start of the experiment of 9th of September is time zero).

3.2.2. Assuming different properties in the two reservoir layers

In the next set of simulations, cases with meaningful combinations of different permeabilities in the two reservoir layers were considered.

Figure 6 compares the pressure response for different permeability combinations between the two layers but assuming the same residual gas saturation of 0.1 (cases 2,5,12 in Table 2). It can be seen that best agreement with data is obtained with similar permeability in the two layers (Case 2) rather than extreme difference between the permeability (Case 12).

Figure 7 in turn, shows a comparison of cases where layer permeabilities are identical but the residual saturations are varied (Cases 2,4,10 and 11 in Table 2). It can be seen that the best agreement with data is obtained in case 4 with lowest residual saturation and worst agreement with case 2, with highest residual saturation.

Figure 8 shows a comparison of cases with moderate and meaningful difference in layer permeabilities, but varying the residual gas saturation (Cases 5,6,7,8 in Table 2). The case 6 (lowest residual saturation in both layers) shows the best agreement with the data, while case 5 (highest residual saturation in both layers) shows the worst agreement.

Overall, the results show that the pressure response of the second hydraulic test is more sensitive to gas residual saturation in the lower reservoir. Gas saturation distribution at various stages of the simulation for two example scenarios (2, with same permeability in the two layers and 12, with order-of-magnitude difference in layer permeabilities) is shown in Figure 9. The figure shows how layer permeability affects the gas distribution in between the reservoirs.

The effect of permeability anisotropy was also tested by comparing anisotropy ratio, horizontal to vertical permeability, of 1 and 3 (Figure 9). Buoyancy effect plays a more important rule when vertical permeability is higher causing vertical migration of the gas to the top of the formation.

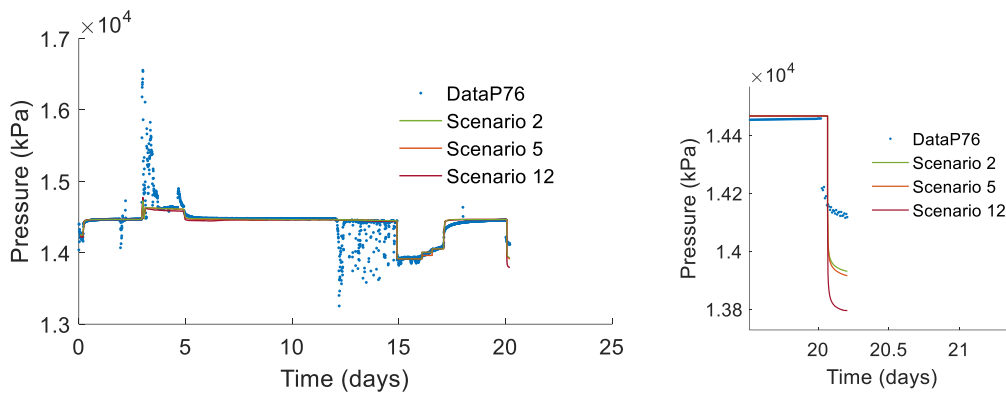


Figure 6. Comparing the simulated pressure with data for different combinations of layer permeability

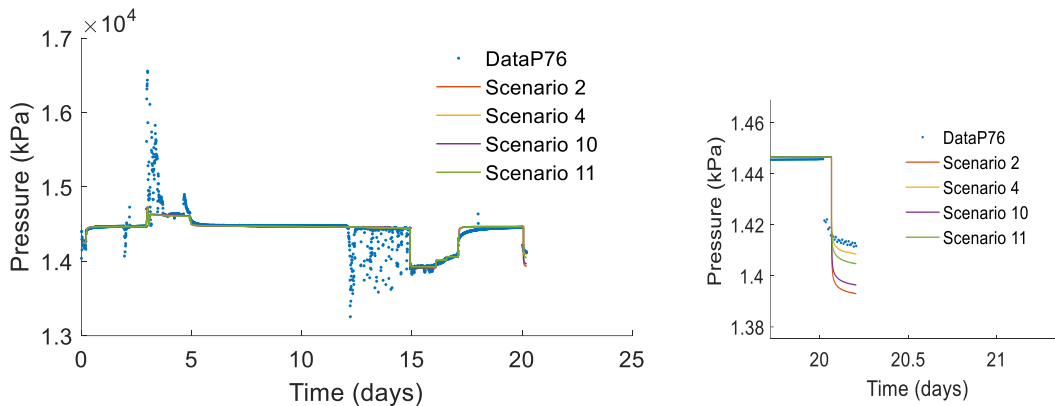


Figure 7. Comparing the simulated pressure with data for different residual gas saturations but same permeability in the two layers

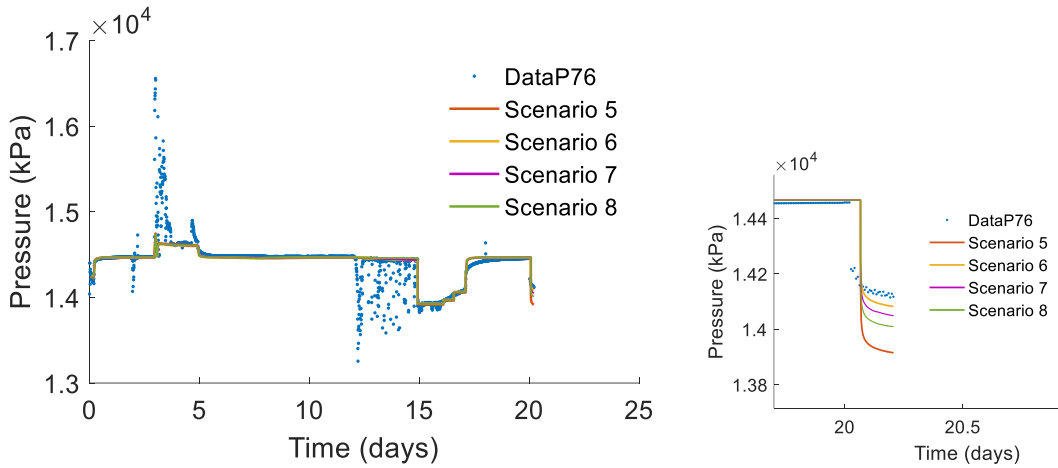


Figure 8. Comparing the simulated pressure with data for models with different permeability and residual saturation in the two reservoir layers

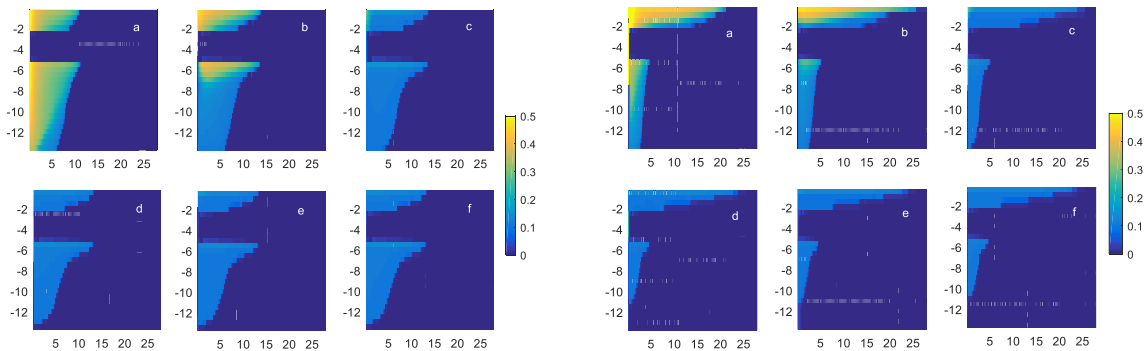


Figure 9. Gas saturation distribution at different stages of the simulation for left) scenario (2) and right) scenario (12): a) after CO₂ injection, b) after rest, c) after self-release, d) after pumping, e) after 2d rest, f) after 2d hydraulic test.

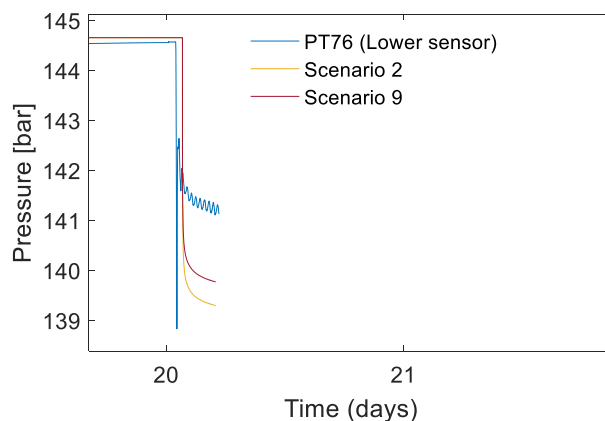


Figure 10. The effect of anisotropy on simulated pressure

3.2.3. Accounting for relative permeability hysteresis

In the previous simulations, the hysteresis effects of wetting and imbibition during CO₂ injection and subsequent withdrawal was not accounted for. Yet, this is a known process to exist. Hingerl et al (2016) provided drainage and imbibition data based on a core sample from the site (Figure 2). These data have been used as basis and hysteresis models with two values of 0.1 and 0.2 for the maximum gas residual saturation (Figure 2) have been tested. Simulation results of the pressure variation (for the second hydraulic test only) are shown in Figure (10). The results show that the hysteretic case with maximum residual saturation of 0.10 shows the best agreement.

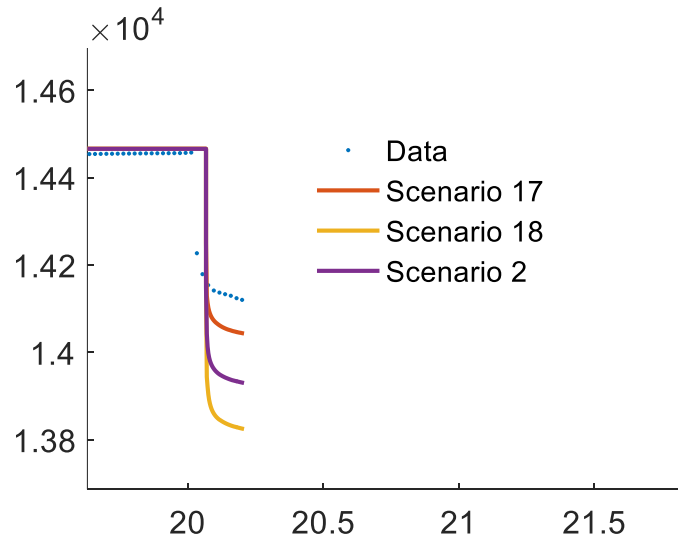


Figure 11. Comparison of pressure response of the second hydraulic test between non-hysteretic and hysteretic relative permeability models with maximum residual gas saturation of 0.1 and 0.2

3.2.4 Modelling the temperature response

Temperature records (sensor PT78) were also used to calibrate/verify the model. Water injection cools down the well's surrounding to about 60 °C. Afterwards, the temperature starts to increase gradually during CO₂ injection. As the processes in the injection well are not modelled in the present study (see Deliverable 4.6 for such models) the temperature of the injected fluids at the reservoir depth is not known and enthalpy of both the injected water and CO₂ was chosen (within the range of meaningful values) so that the simulation results would best fit the measured temperature data. In the case of CO₂ injection, we tested several

injection temperatures and enthalpies of the injected fluid was chosen so that the temperature at the end of the injection matches the data (injection temperature temperature 63 °C

in Figure 12a). Capturing the gradual temperature increase during CO₂ injection is, however, more challenging as using a single injection temperature causes an abrupt jump in temperature response. This behavior was not sensitive to thermal properties of the sand layers and the wall (see Table 3) (Figure 12b) or to gas residual saturations and heterogeneity (Figure 12c). It was also insensitive to mesh discretization (not shown here).

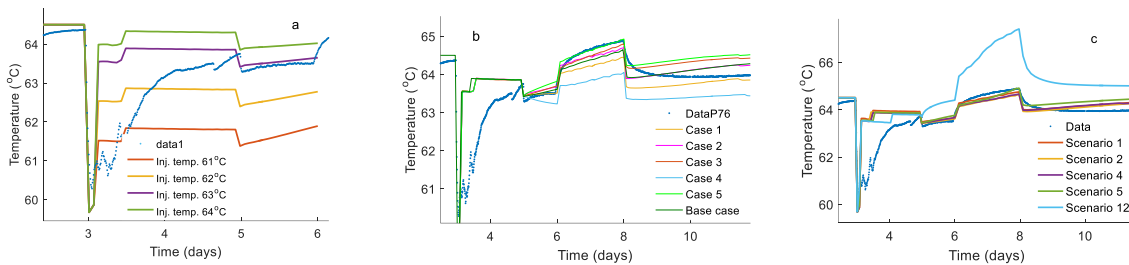


Figure 12. Simulation of the temperature variation: a) the effect of injection temperature, b) the effect of thermal properties, c) the effect of gas residual saturation and layered heterogeneity

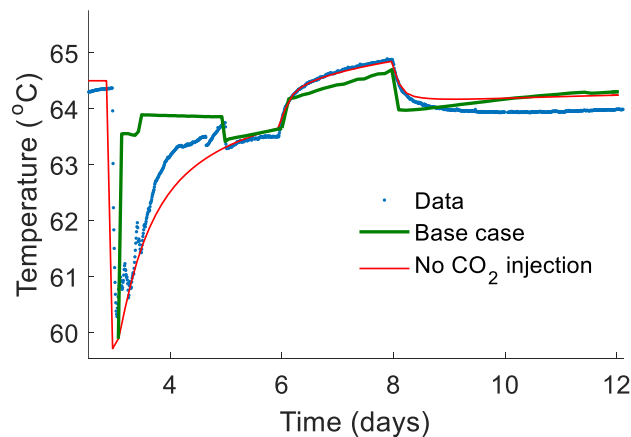


Figure 13. Simulation of the temperature variation without CO₂ injection

Table 3. Table of the thermal properties tested in the simulations

	Sand heat conductivity (wet condition) (W/m oC)	Sand heat conductivity (dry condition) (W/m oC)	Sand heat capacity	Well heat conductivity (wet condition) (W/m oC)	Well heat conductivity (dry condition) (W/m oC)	Well heat capacity
Base Case	6	1.8	870	6	1.8	870
Case 1	2	1.8	870	1.2	1.8	870
Case 2	6	0.1	870	6	0.1	870
Case 3	6	10	870	6	10	870
Case 4	6	1.8	8700	6	1.8	8700
Case 5	10	1.8	870	6	1.8	870

3.2.5 Modified conceptual model

The previous results indicate that more CO₂ is going to the upper layer than the permeability difference would indicate. In this study we are not using a detailed wellbore model that would allow investigating the dynamics of CO₂ distribution inside the injection well. This is investigated in Deliverable 4.6 and indications are also given in Rasmusson et al. (2015), which shows that in a layered CO₂ injection system more gas goes into the upper layer than the permeability difference would indicate. To allow the gas to enter more the upper layer, we consider an assumption that would limit the amount of the gas that could enter the lower sandstone A. One explanation could be that the water which filled the well before the CO₂ injection might have accumulated in the bottom right after starting of the gas injection which could reduce the relative permeability of the gas and could have blocked the gas from entering the lower formation.

To simulate this scenario, we tested a case where permeability of the lower 9 m of the injection well during CO₂ injection and heating process was 3 orders of magnitudes smaller than the permeability of the upper 5m of the well (Figure 14). The simulations results show an improvement in fitting both the temperature (Figure 15a) and pressure (Figure 15b) response. Figure 16 compares the hysteretic and non-hysteretic relative permeability functions with this new assumption. Our results show that if hysteresis in relative permeability and capillary functions was neglected, only a model with low residual gas saturation (Scenarios 4 and 15) can closely match the pressure data.

Considering hysteresis in the characteristic curves, a model with maximum residual gas saturation of 0.1 and the assumption of lower permeability at the lower part of the well (Scenario 19) shows a good agreement with all the data. Gas saturation distribution for this scenario at different stages of the simulation is shown

in Figure 17. Table 4. lists the tested scenarios that match the pressure data best. Column ΔP represents the difference between pressure data and simulations at the end of the second hydraulic test. The total amount of CO₂ stored at both layers after the second hydraulic test have specified as well. Simulations that have a good agreement with temperature data are highlighted in green.

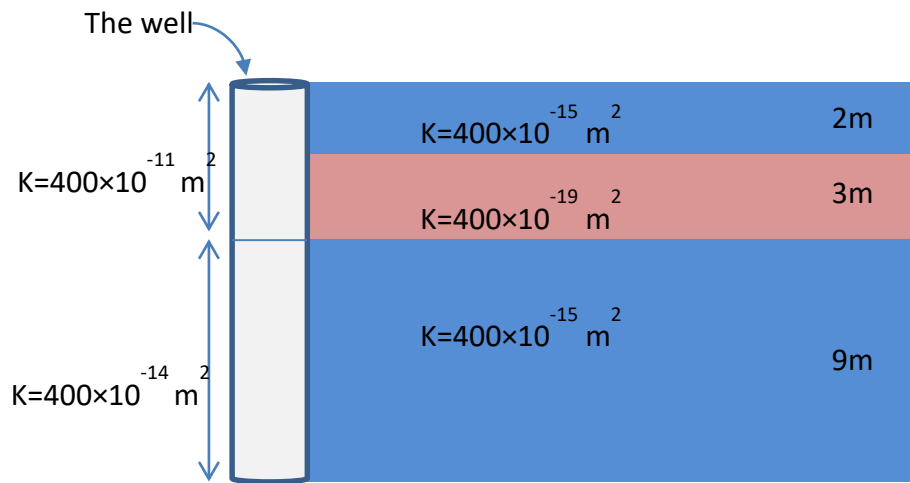


Figure 14. The conceptual model with lower permeability in lower 9m part of the well. This assumption was applied only during CO₂ injection and heating.

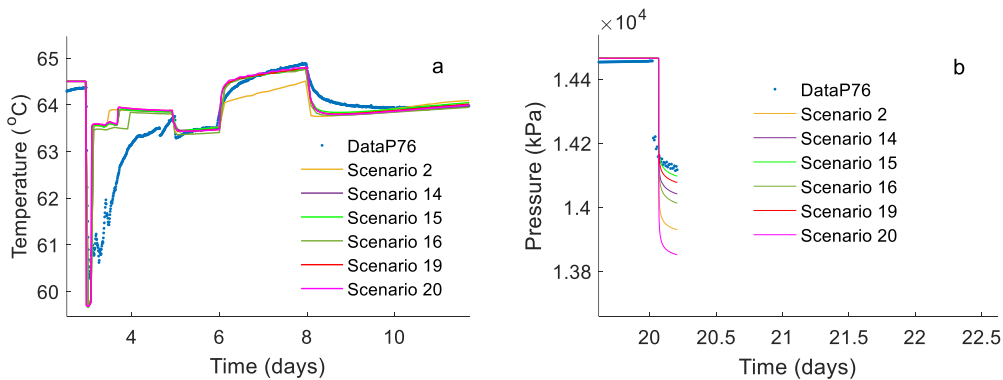


Figure 15. a) Temperature and b) pressure simulations with modified model

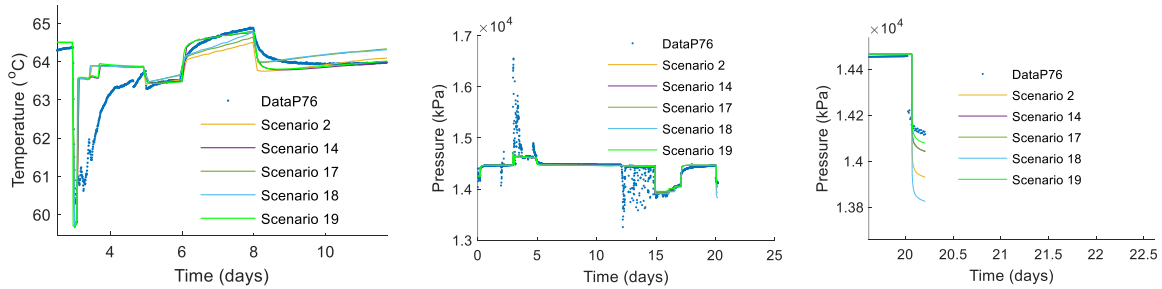


Figure 16. Comparing hysteretic and non-hysteretic models for the modified model

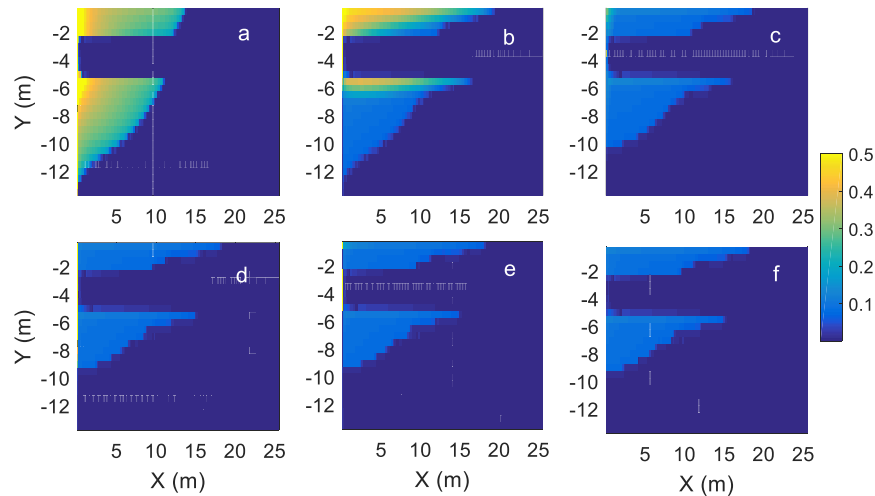


Figure 17. Gas saturation distribution at different stages of the simulation for scenario (19) a) after CO₂ injection, b) after rest, c) after self-release, d) after pumping, e) after 2d rest, f) after 2d hydraulic test.

Table 4. Comparing remained CO₂ mass in both reservoirs after the second hydraulic test, sorted based on the best fitting scenario

	Mass in Sand A	Mass in Sand W	Total	ΔP (bar)
Scenario 15	16	23	39	0.23
Scenario 4	19	13	32	0.3
Scenario 6	13	20	33	0.4
Scenario 19	20	24	45	0.5
Scenario 2	31	17	48	1.4

3.3 Conclusions

Overall, the modeling of the Residual Trapping Experiment I indicated that relatively small amounts of CO₂ were present in the layer facing the sensors in the borehole. The best overall agreement between the model and the measured data was obtained by assuming a 400 mD permeability in both layers A and W, along with hysteretic relative permeability functions and assuming that there is a reduced flow of CO₂ to the lower reservoir layer, due to blocking of the gas flow in the well by water from earlier water injection phases. The resulting calibrated values are in good agreement with other measurements carried out on the site. The estimated residual saturation is somewhat below the value determined from the laboratory experiments.

4. Modeling of the Residual Trapping Experiment II

4.1 Test sequence

The test sequence of RTE II shown in Figure 18. Again, extensive presentation of the data is given in Deliverable 2.3 – 2.4 (Part 1) and will not be repeated here. The key data used for model calibration included the down-hole pressure and temperature measurements, measured fluid flow rates and U-tube fluid samples, especially concerning the partitioning tracer Kr recovery in the characterization tests before and after creating the residually trapped zone.

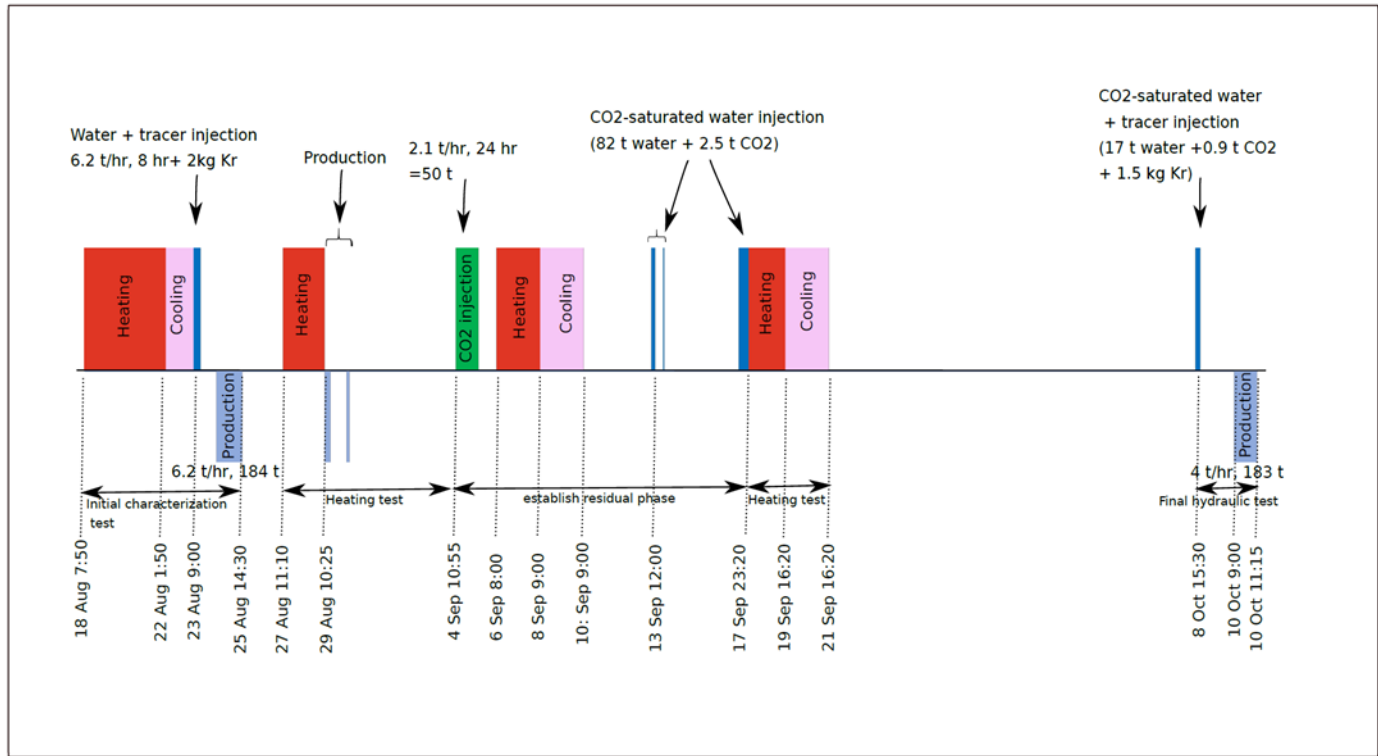


Figure 18. Test sequence of Residual Trapping Experiment II

4.2 Modeling the first phases of the experiment

Based on the results from modeling the Residual Trapping Experiment I in the previous section, the modified conceptual model (Section 3.2.3) was used to model the data from the Residual Trapping Experiment II. As for RTE I, the homogeneous sandstone layers with permeability of 400 mD could well satisfy the pressure response of the first hydraulic test during the abstraction (Figure 19). It also matches the pressure drops during the next production events on 29th and 30th August. The very high pressure response in the data during the first water injection can be related to accumulation of mud next to the well due to previous abstraction processes.

Figure 20 shows the data and simulation results of the injection and production of 2 kg Kr as a partitioning tracer during the first characterization test on 23 to 25th of August. The blue dots are Krypton concentrations in the liquid phase, obtained and inverted from U-tube samples (see Deliverable 2.3-2.4, Part 1). The first peak shows simulation results of the tracer concentration in the well during the injection and the second

peak the tracer recovery. The agreement is remarkably good considering that no model calibration had been carried out after the analysis of RTE I.

Pressure changes during the CO₂ injection between 4-5th of September, are shown in Figure 21. During this stage, 50 tons of supercritical CO₂ has been injected. Injection rates and the amounts of injected fluids are also summarized in Deliverable 2.3-2.4.

The state of residual trapping was in RTE II created by CO₂-saturated water injection. However, before CO₂-saturated water injection on 13th September, the well first was opened to atmospheric pressure, allowing free CO₂ to escape like in the RTE I. Like for the previous experiment, this process was modeled by defining the pressure in the well grids at given times, as measured (Figure 20). The pressure-drop in the well causes a pressure gradient and results in the flow of fluids towards the well.

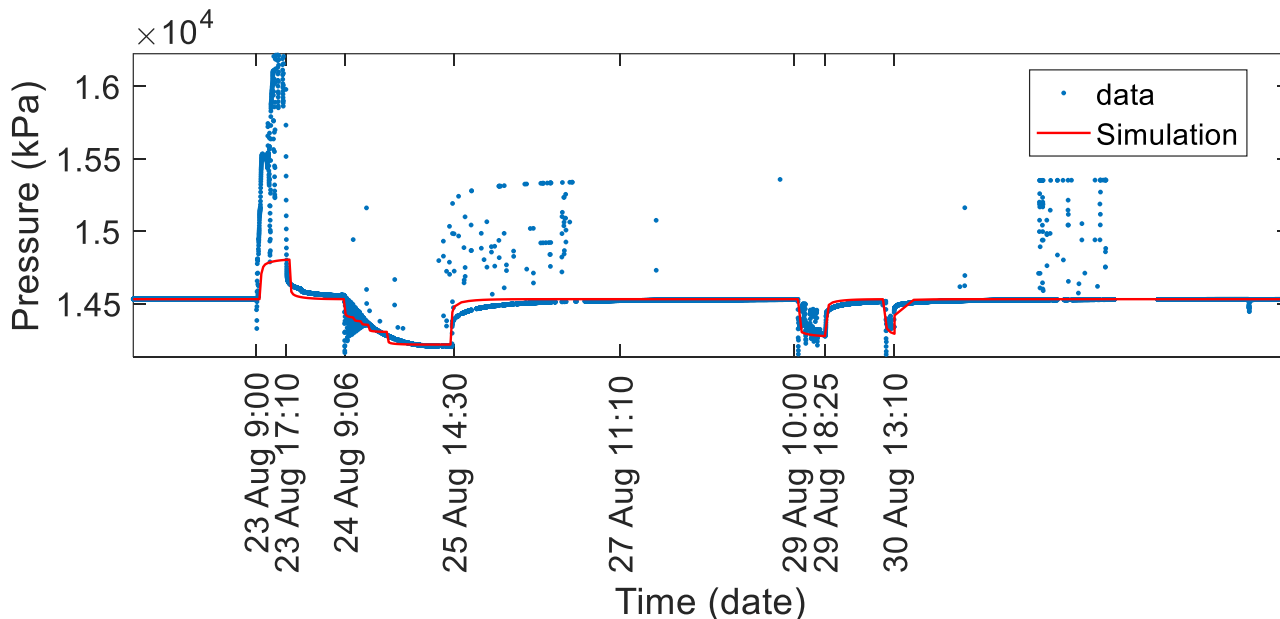


Figure 19. Simulation results of the pressure 1 m below the shale layer during the first hydraulic test

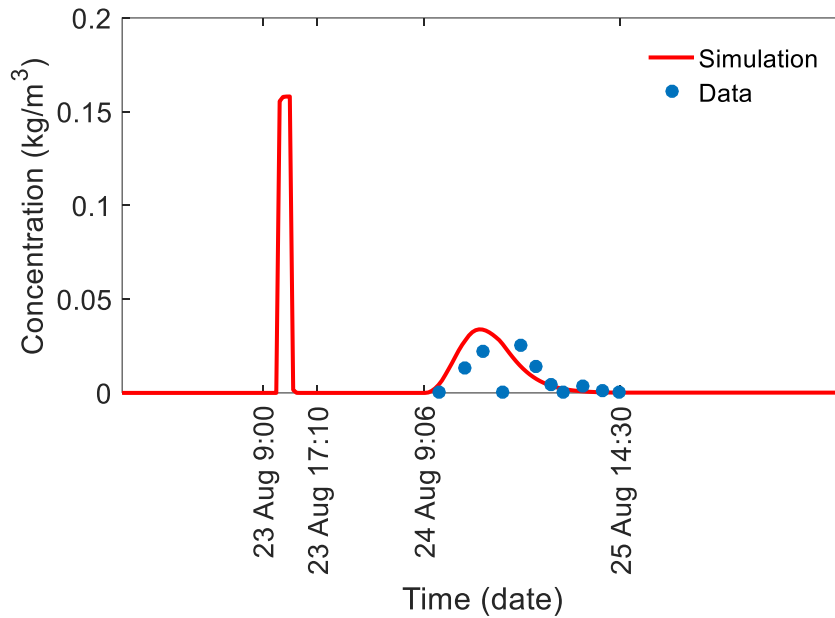


Figure 20. U-tube data on Krypton and simulation results of the tracer concentration in liquid phase during the abstraction

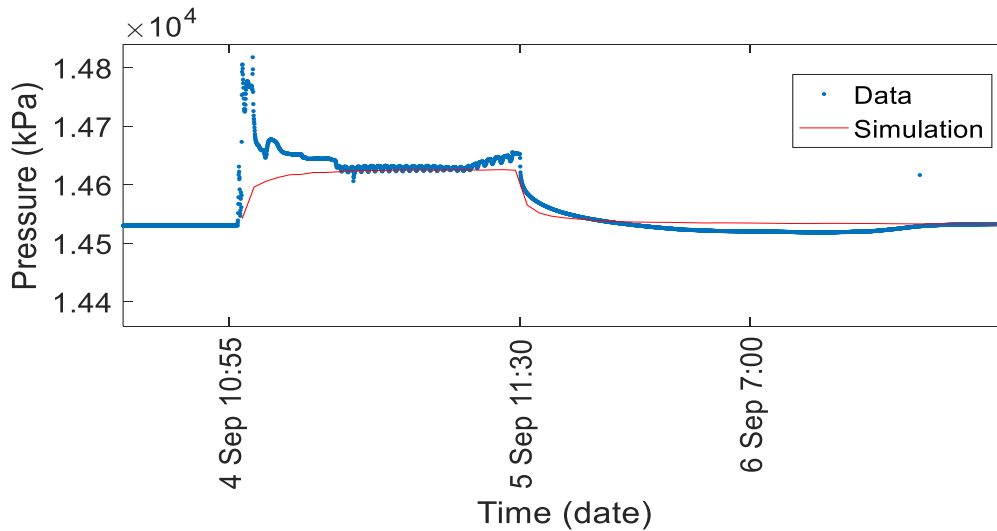


Figure 21. Simulated and measured downhole pressure during CO₂ injection

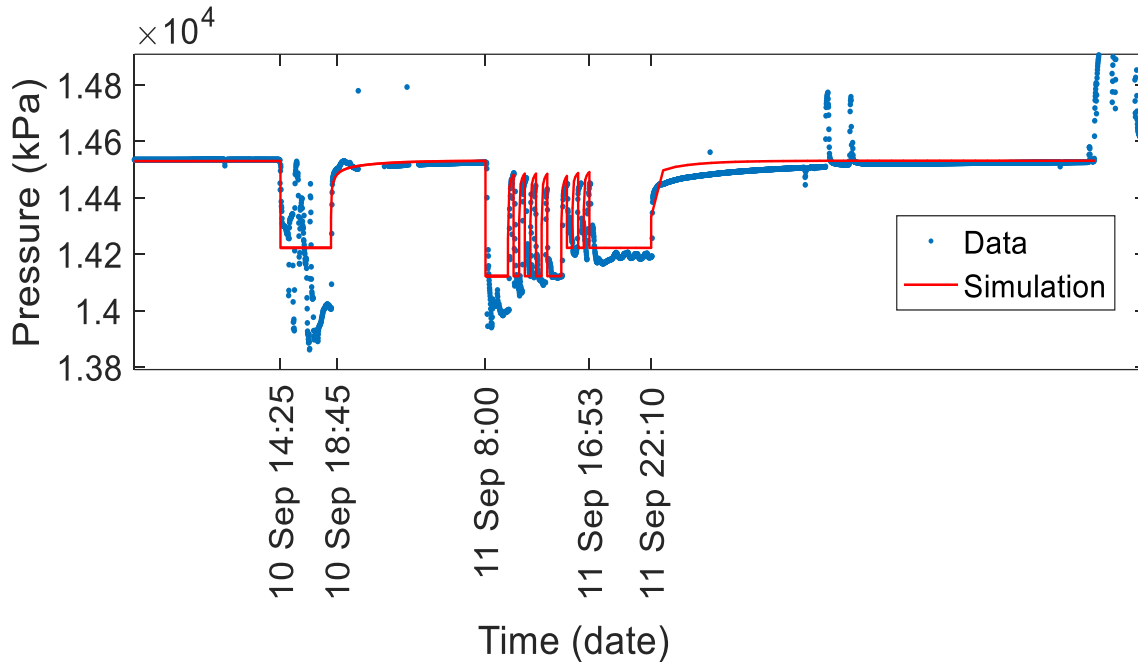


Figure 21. Pressure simulation during self-release

4.3 Modelling phases after the CO₂ saturated water injection

4.3.1 The effect of relative permeability function

Coupled wellbore modeling (applied in a separate study, in Deliverable 4.6) has suggested that the self-release phenomenon after the well opening can be related to gas exsolution in the reservoir which in turn can dramatically reduce the mobility of gas and liquid phases. In order to take into account this effect, two sets of relative permeability functions were used to model the self-release and processes that followed afterwards. These two functions that are shown in Figure 22 which shows the original Brooks-Corey functions and the reduced permeability functions in which gas relative permeability was assigned to zero and liquid relative permeability was defined so that the liquid phase is mobile only when the gas saturation is very low.

The effect of this assumption is shown in Figure 22 where the pressure responses during CO₂-saturated water injection for both relative permeability curves are compared. Simulated pressure response during CO₂-saturated water injection agrees well with the data on day 13th September. However, it is somewhat lower than the recorded pressure data on 14th and especially on 17th September. The assumption of reduced relative permeability slightly improves the simulation results but the reason for the difference between data and simulation is still not known and investigations continue to address the discrepancy. Simulated pressure

increases during the second tracer injection test (Figure 24.) is also less than the recorded data at the sensor.

Our model with residual gas saturation of 0.05 matches the pressure drop during the abstraction (Figure 24) and this result is independent of the relative permeability function. Simulation results of the tracer recovery with both functions are shown in Figure 25. Partitioning coefficient for Krypton was chosen based on (Zhang et al. 2011) and contains uncertainties. While the overall shape and arrival pattern of the modelled and measured tracer breakthrough are in seeming good agreement, indicating appropriate amounts of CO₂ in the formation being modelled, the breakthrough of the tracer in the simulations is almost 4 hours ahead of the first non-zero concentration obtained from U-tube sampling. At the time of writing this report, work continues to improve the model agreement with data.

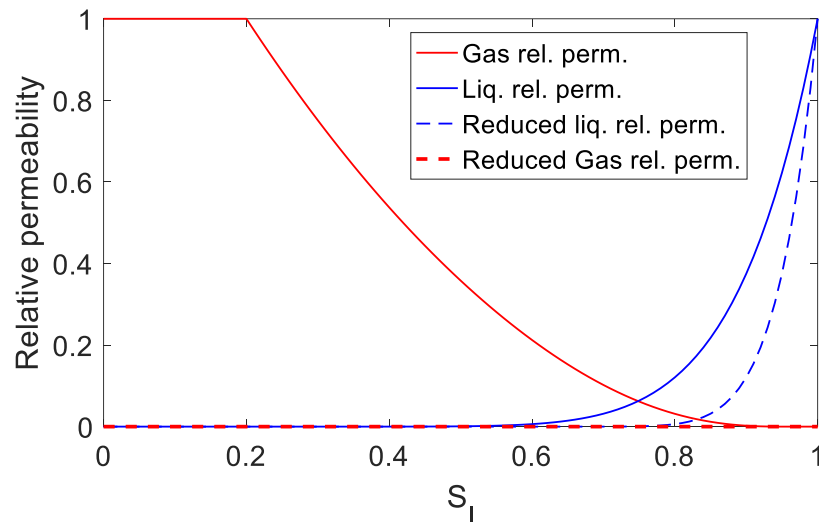


Figure 22. Relative permeability curves used for the simulations

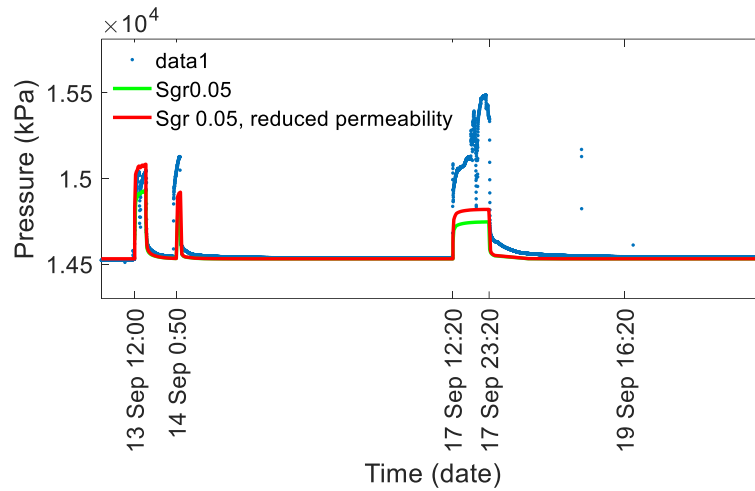


Figure 23. Pressure simulations, comparing the effect of relative permeability curves

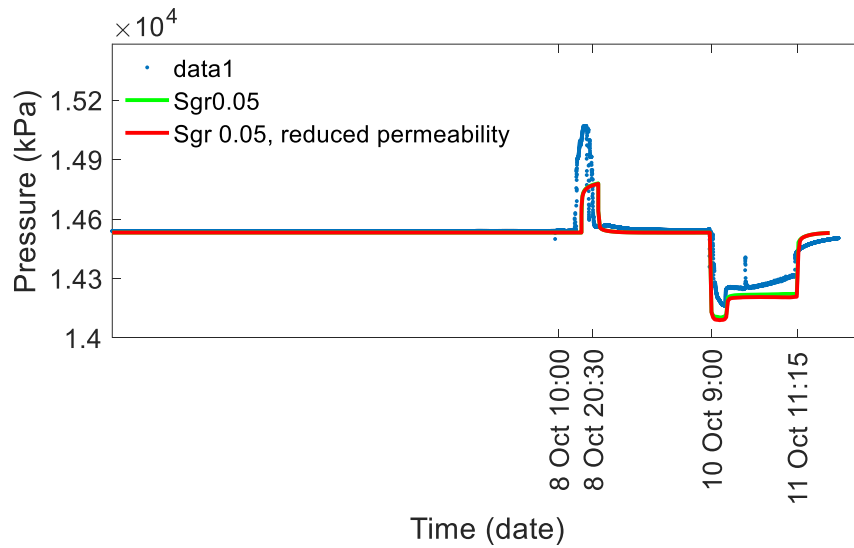


Figure 24. Pressure simulation of the second hydraulic test, comparing the effect of relative permeability functions

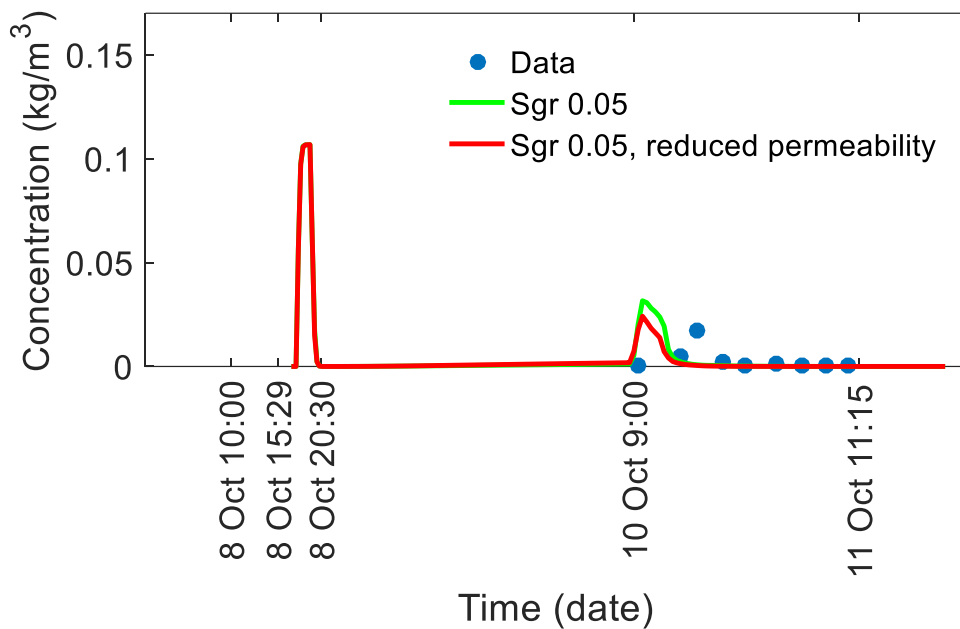


Figure 25. Concentration of the tracer in the well, comparing the effect of relative permeability functions

4.3.2 Hysteretic model

Gas saturation distribution at different stages of the experiment based on non-hysteretic and hysteretic models (from Chapter 3) are shown in Figures 26 and 27, respectively. Pressure responses for the same models during CO₂-saturated water injection are presented in Figure 28. It can be seen that even if the modelled gas saturation distributions for hysteretic and non-hysteretic simulations are different (Figures 26-27) the pressure response in the sensor is very similar for both cases (Figure 28). This indicates that the pressure response in the sensor is not capturing the gas distribution in the formation in detail, and further studies should address this issue in more detail. The simulated tracer concentration during the second hydraulic test for both the non-hysteretic ($S_{gr}=0.05$) and the hysteretic model (with $S_{grmax}=0.1$) are shown in Figure 29. The hysteretic and non-hysteretic models show similar behavior and both predict slightly too fast arrival.

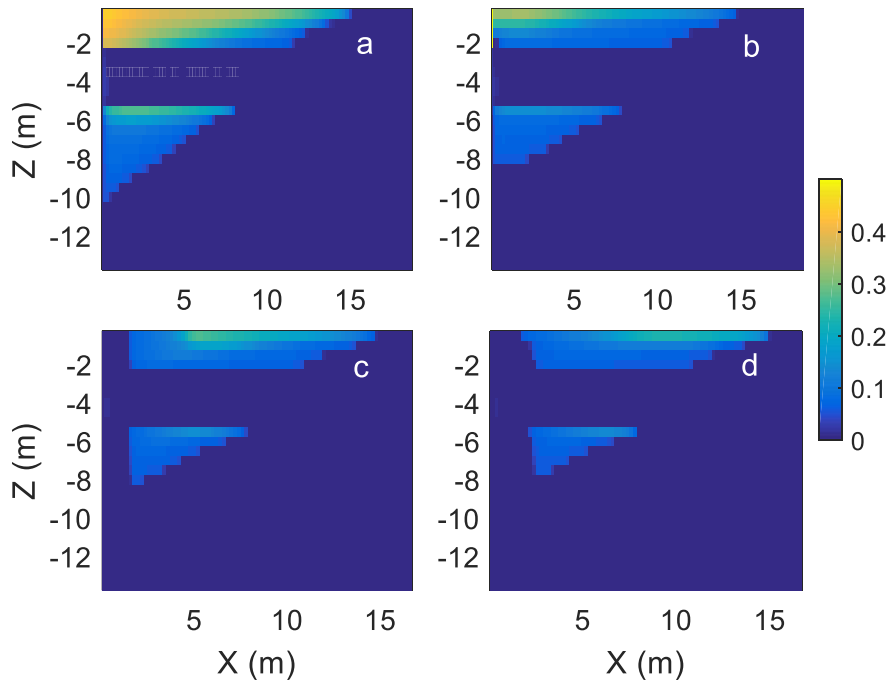


Figure 26. Simulated gas saturation distribution for the base scenario at: a) beginning of the self-release, b) end of the self-release, c) after the first CO₂-saturated water injection on 13th September, d) after the third CO₂-saturated water injection on 17th September.

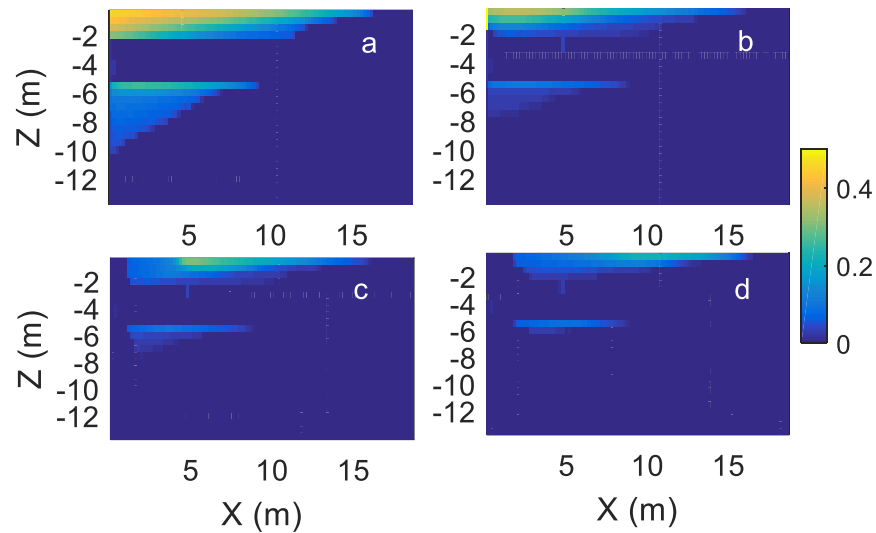


Figure 27. Simulated gas saturation distribution for the hysteresis model at: a) beginning of the self-release, b) end of the self-release, c) after the first CO₂-saturated water injection on 13th September, d) after the third CO₂-saturated water injection on 17th September.

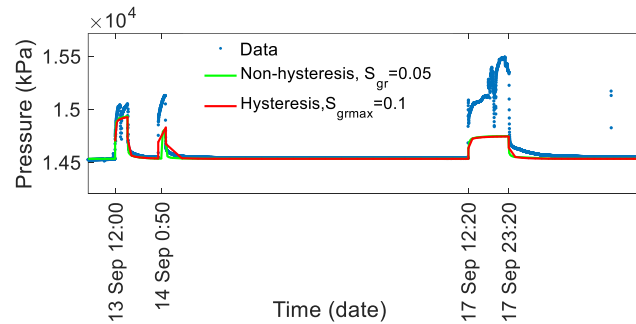


Figure 28. Simulation of the pressure response during CO₂-saturated water injection, comparing the effect of hysteresis and non-hysteresis relative permeability

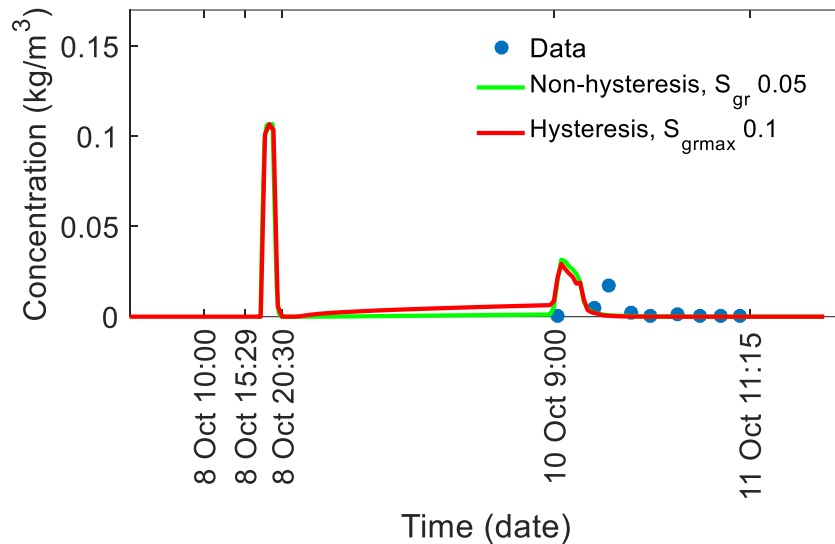


Figure 29. Concentration of the tracer in the well, comparing the effect of hysteresis and non-hysteresis relative permeability

4.4 Conclusions

At the time of writing this report, the modeling analysis of RTE II is still underway, due to timing issues in carrying out the experiment and data transfer and the time of final reporting of TRUST. The partitioning tracer recovery in the RTE II experiments was successful and the results form a good basis for verifying and complementing the results from RTE I. The early part of RTE II was almost perfectly matched with the model calibrated in RTE I, without any adjustments of the model, which is very encouraging indeed. The later parts of the experiment, and the recovery of the tracer when residual CO₂ is present in the formation, show also similar tracer recoveries between the model and the experiment, thereby indicating that the level of residual trapping estimated from RTE I is correct. The test sequence (including the coupled processes of well-reservoir interaction) during the injection of CO₂ saturated water and the partitioning tracer are, however, complex and presently – at the time of writing this report – work continues to finalize the model calibration for a more perfect agreement in tracer arrival for the second partitioning test.

5. Conclusions

This Deliverable presents the first model interpretations of Heletz, Israel residual trapping experiments, the Residual Trapping Experiment I (RTE I) carried out in September 2016 and the Residual Trapping Experiment II (RTE II) carried out in August to November 2017. The experiments are based on the principle of a combination of hydraulic, thermal and/or tracer tests before and after creating the residually trapped zone of CO₂ and using the difference in the responses of these tests to estimate the in-situ residual trapping. The first experiment, RTE I, is based on hydraulic withdrawal tests before and after the creation of the residually trapped zone. The residually trapped zone was also created by fluid withdrawal, by first injecting CO₂, then withdrawing fluids until CO₂ was at residual saturation. In the second experiment, RTE II, the main characterization method was injection/withdrawal of water and partitioning tracers, whose recovery with and without residually trapped CO₂ in the formation was compared. In this second experiment the residually trapped zone was created by first injecting CO₂ and then injecting water saturated with CO₂ to push away the mobile CO₂ and leaving the residually trapped zone behind.

Here, the experimental results of **RTE I** have been modelled first. A simplified analytical model was first used for guidance, followed by 'full-physics' modeling with the TOUGH2 simulator, where all the data (temperature, pressure, flow rates, two-phase flow behavior etc.) were matched. Comprehensive calibration procedure led to a best-estimate of the test behavior, suggesting an in-situ residual saturation of 0.1, including a hysteretic behavior in the relative permeability functions, similar properties in the two reservoir layers and preference of the CO₂ to enter the upper layer.

The 'full-physics' model calibrated with RTE I was then used to model the later RTE II. Without any further calibration, the model calibrated by RTE I showed excellent agreement even for this second experiment, for the early parts of RTE I until the time of CO₂ saturated water injection. saturated results showed a perfect agreement for the early parts of the experiment (prior to establishing the residually trapped zone) and relatively good agreement even with the later parts, with residually trapped CO₂ in the formation. In particular, the amount of the tracer partitioned into CO₂ was well captured with the earlier calibrated model, without any further adjustments, indicating a similar estimate of residually trapped CO₂ than from RTE I. Due to time considerations - in terms of the data from RTE II becoming available for modeling - the modeling of RTE II is still in progress at the time of final reporting of TRUST project and writing of this deliverable. As of the results so far it seems, however, that the conclusions from RTE I give a good estimation of the residual trapping at Heletz.

6. References

- Benson, S.M. et al., 2015. Relative permeability for multi-phase flow in CO₂ storage reservoirs. Part II: resolving fundamental issues and filling data gaps.
- Dance, T. & Paterson, L., 2016. Observations of carbon dioxide saturation distribution and residual trapping using core analysis and repeat pulsed-neutron logging at the CO₂CRC Otway site. *International Journal of Greenhouse Gas Control*, 47, pp.210–220. Available at: <http://dx.doi.org/10.1016/j.ijggc.2016.01.042>.
- Doughty, C., 2013. User's Guide for Hysteretic Capillary Pressure and Relative Permeability Functions in TOUGH2.
- Hingerl, F.F. et al., 2016. Characterization of heterogeneity in the Heletz sandstone from core to pore scale and quantification of its impact on multi-phase flow. *International Journal of Greenhouse Gas Control*, 48, pp.69–83. Available at: <http://dx.doi.org/10.1016/j.ijggc.2015.12.037>.
- Niemi, A. et al., 2016. Heletz experimental site overview, characterization and data analysis for CO₂ injection and geological storage. *International Journal of Greenhouse Gas Control*, 48, pp.3–23. Available at: <http://dx.doi.org/10.1016/j.ijggc.2015.12.030>.
- Oldenburg, C.M. et al., 2004. EOS7C Version 1.0: TOUGH2 Module for Carbon Dioxide or Nitrogen in Natural Gas (Methane) Reservoirs. *Lbnl-56589*, (March), pp.1–53.
- Paterson, L., Boreham, C., Bunch, M., Dance, T., Ennis-King, J., Freifel, B., Haese, R., Jenkins, C., Raab, M., Singh, R and Stalker L. (2014) CO₂CRC Otway Stage 2B residual saturation and dissolution test. In PJ. Cook, editor. *Geologically Storing Carbon: Learning from the Otway Project Experience*. Chapter 17. Pp 343-380. CSIRO publishing. Melbourne 2014.
- Pruess, K., 2005. ECO₂N: A TOUGH2 Fluid Property Module for Mixtures of Water, NaCl, and CO₂. *Contract*, (June), pp.1–76.
- Pruess, K., Oldenburg, C. & Moridis, G., 1999. TOUGH2 USER'S GUIDE, VERSION 2.
- Rasmusson, K. et al., 2014. Analysis of alternative push-pull-test-designs for determining in situ residual trapping of carbon dioxide. *International Journal of Greenhouse Gas Control*, 27, pp.155–168. Available at: <http://dx.doi.org/10.1016/j.ijggc.2014.05.008>.
- Rasmusson, K. et al., 2015. Distribution of injected CO₂ in a stratified saline reservoir accounting for coupled wellbore-reservoir flow. *Greenhouse Gases: Science and Technology*, 5(4), pp.419–436. Available at: <http://doi.wiley.com/10.1002/ghg.1477> [Accessed March 10, 2018].
- Zhang, Y. et al., 2011. Single-well experimental design for studying residual trapping of supercritical carbon dioxide. *International Journal of Greenhouse Gas Control*, 5(1), pp.88–98.

APPENDIX A

Preliminary analysis of hydraulic test response of RTE I

Updated 2017-02-23 Zhibing Yang and Auli Niemi

1. The test sequence

The Heletz site in Israel has been developed for scientifically motivated CO₂ injection experiments with the objective of improving our understanding of the fate of the geologically stored CO₂, including processes of CO₂ spreading and trapping in geological formations [Niemi et al., 2016]. In September 2016, a test sequence was carried out. The sequence included hydraulic tests, CO₂ injection, passive release of CO₂ from the well, and active production of CO₂ (see Figure 1).

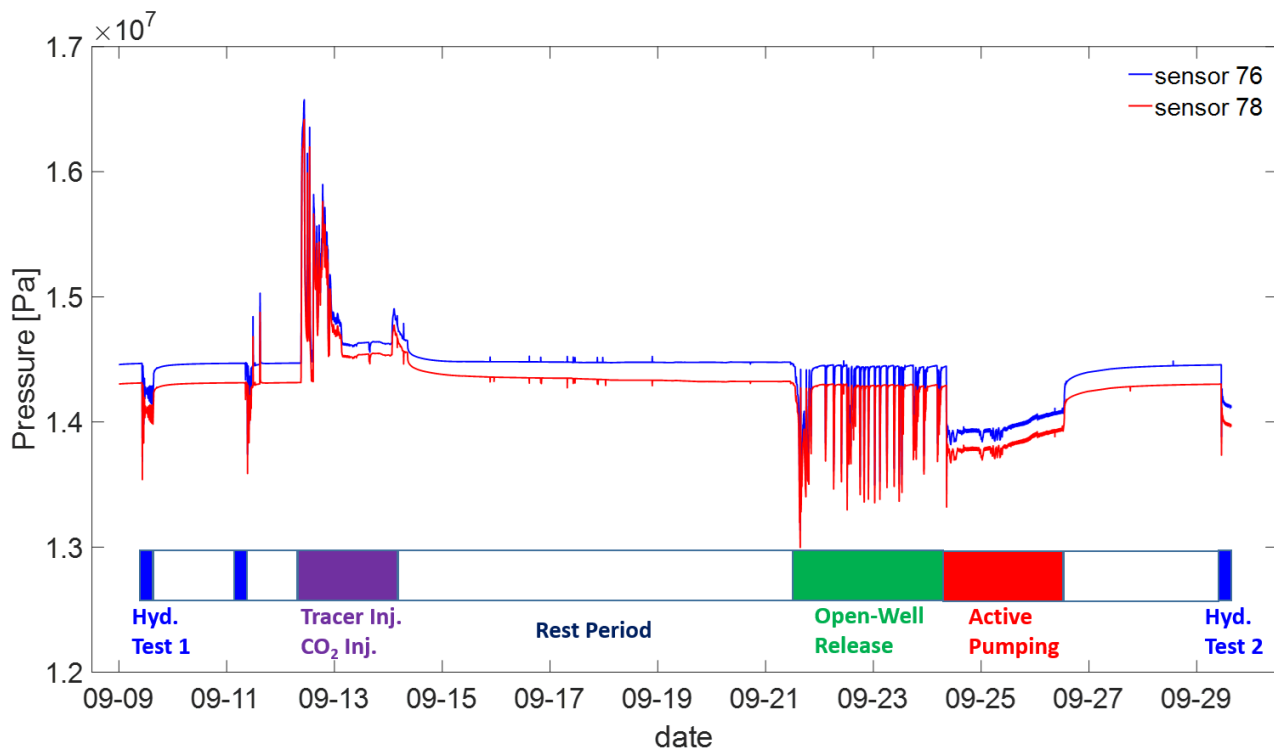


Figure 1. The test sequence (September 2016) and pressure series for Sensors 76 (at depth 1617.35m) and 78 (at depth 1632.91m). The x axis ticks mark the start (00:00) of the day.

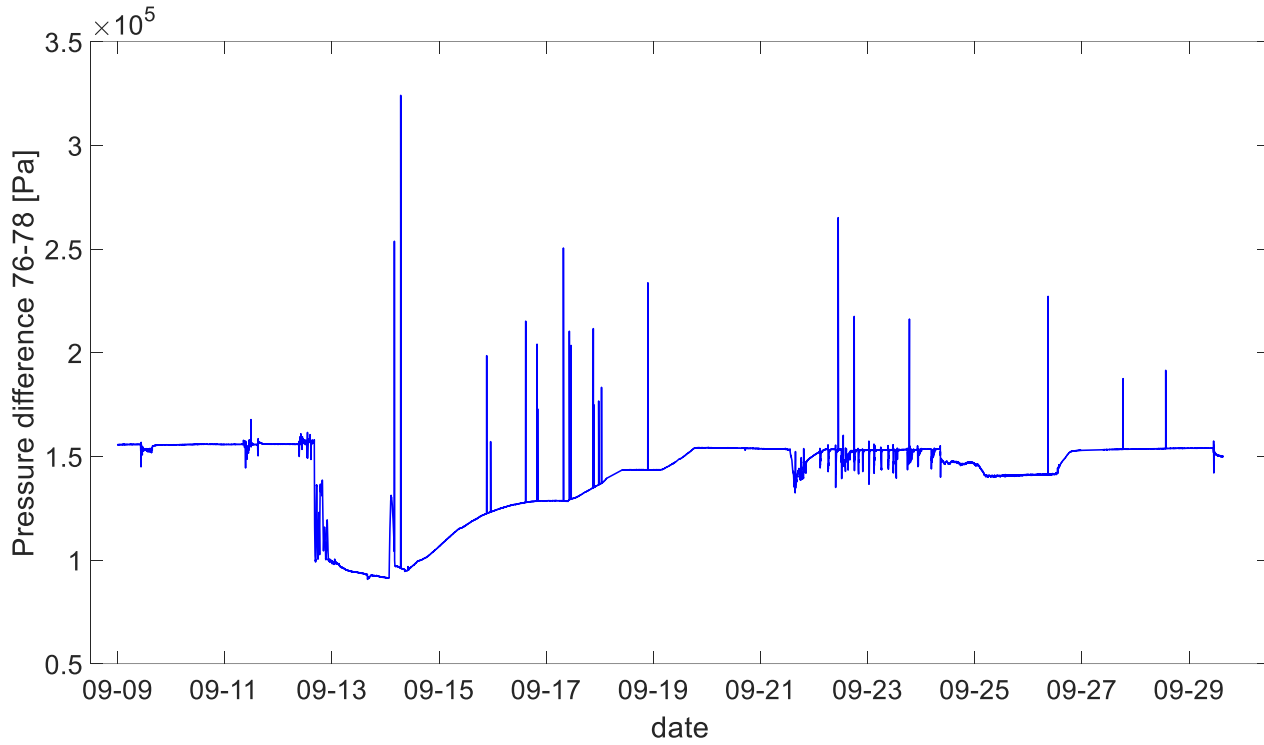


Figure 2. Pressure difference between Sensor 76 and 78.

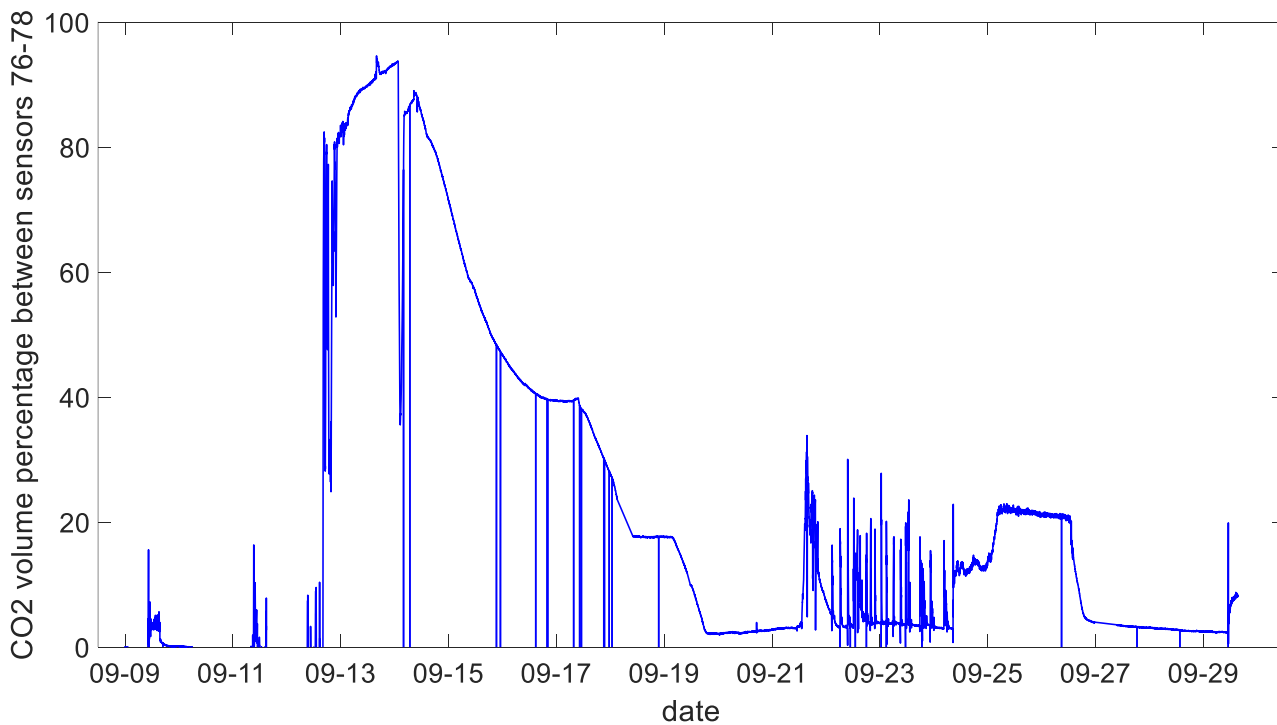


Figure 2. Interpreted gas volume percentage between Sensor 76 and 78.

2. Analysis of the hydraulic tests before and after CO₂ injection

As a preliminary analysis, we use the Theis solution which, written in terms of pressure change ΔP at radial distance r and time t for an ideal aquifer, is

$$\Delta P = P - P_0 = \frac{Q\mu_b}{4\pi kb} \int_u^\infty \frac{e^{-u}}{u} du \quad (1)$$

where

$$u = \frac{r^2 S \mu_b}{4tk\rho_b gb} \quad (2)$$

In eqs. (1-2), P is the transient pressure, P_0 is the initial pressure, Q is the volumetric flow rate (negative for pumping), k is the horizontal permeability of the reservoir, S is the storativity of the reservoir, b is the thickness of the reservoir, ρ_b is the density of the native brine, μ_b is the viscosity of the brine. The storativity is calculated by:

$$S = \rho_b gbn(c_w + c_p) \quad (3)$$

where n is the porosity, c_w is the water compressibility ($4.5 \times 10^{-10} \text{ Pa}^{-1}$), c_p is the pore compressibility. If $c_p = 0$, equation (3) gives a lower bound $S \approx 1 \times 10^{-5}$.

We assume (1) a fully penetrated well with respect to the target reservoir and (2) the reservoir is horizontal, homogeneous, and confined, and has uniform thickness. Permeability anisotropy is not considered. The effect of wellbore storage is neglected. Skin effect is not included.

It is necessary to evaluate the appropriateness of some of these assumptions. The effect of vertical anisotropy should be small for a thin, confined layer with a well fully perforated along the reservoir thickness. The wellbore storage affects the early-time pressure response but not the late-time response during a pumping period. In addition, water has a low compressibility and the pressure drop is very small (<1% of the reservoir pressure); thus, the wellbore storage effect may not be significant. Nevertheless, a more detailed analysis regarding these assumptions can be helpful for the situation at Heletz.

The parameters used for the analytical solution are listed in Table 1. The most uncertain parameters are the pore compressibility and the permeability of the reservoir rock. A plausible range for the pore compressibility of sandstone at confining stress of 15 bars is $5 \times 10^{-10} \sim 5 \times 10^{-9} \text{ Pa}^{-1}$. We vary the permeability and the pore compressibility to try to match the pressure data. Note that at this stage, we do not consider

the permeability reduction due to presence of CO₂ in the calculations of pressure response. We do NOT attempt to fit the pressure sequences, since we do not know the effect of injected CO₂ on the hydraulic test and fitting to individual sequences is non-unique given multiple uncertain parameters.

Table 1

Parameter used for pressure analysis

<i>Parameters</i>	<i>Values</i>
Porosity	0.25
Density of brine [kg/m ³]	1050
Viscosity of brine [cP]	0.5
Conductive thickness [m]	9
Water compressibility [Pa ⁻¹]	4.5×10 ⁻¹⁰
Well radius [cm]	2.83
Flow rate [m ³ /hr]	4.9 (Sept 9) and 7.3 (Sept 29)
Pore compressibility [Pa ⁻¹]	5×10 ⁻¹⁰ - 5×10 ⁻⁹
Permeability [mD]	500 - 735

Figure 3 shows that the pressure calculated with the lower permeability of 450 mD tends to better match the measured data. This is assuming no effect of residual CO₂ during the second test on 29th September. If we account for the effect of residual CO₂ by reducing the permeability for the second test, the analytical solution would give an even larger pressure drop (i.e., larger deviation from the data). This preliminary result indicates low levels of CO₂ present in the system during the second hydraulic test. To fully resolve the issue of presence of CO₂, a more detailed analysis with additional data and constraints is needed.

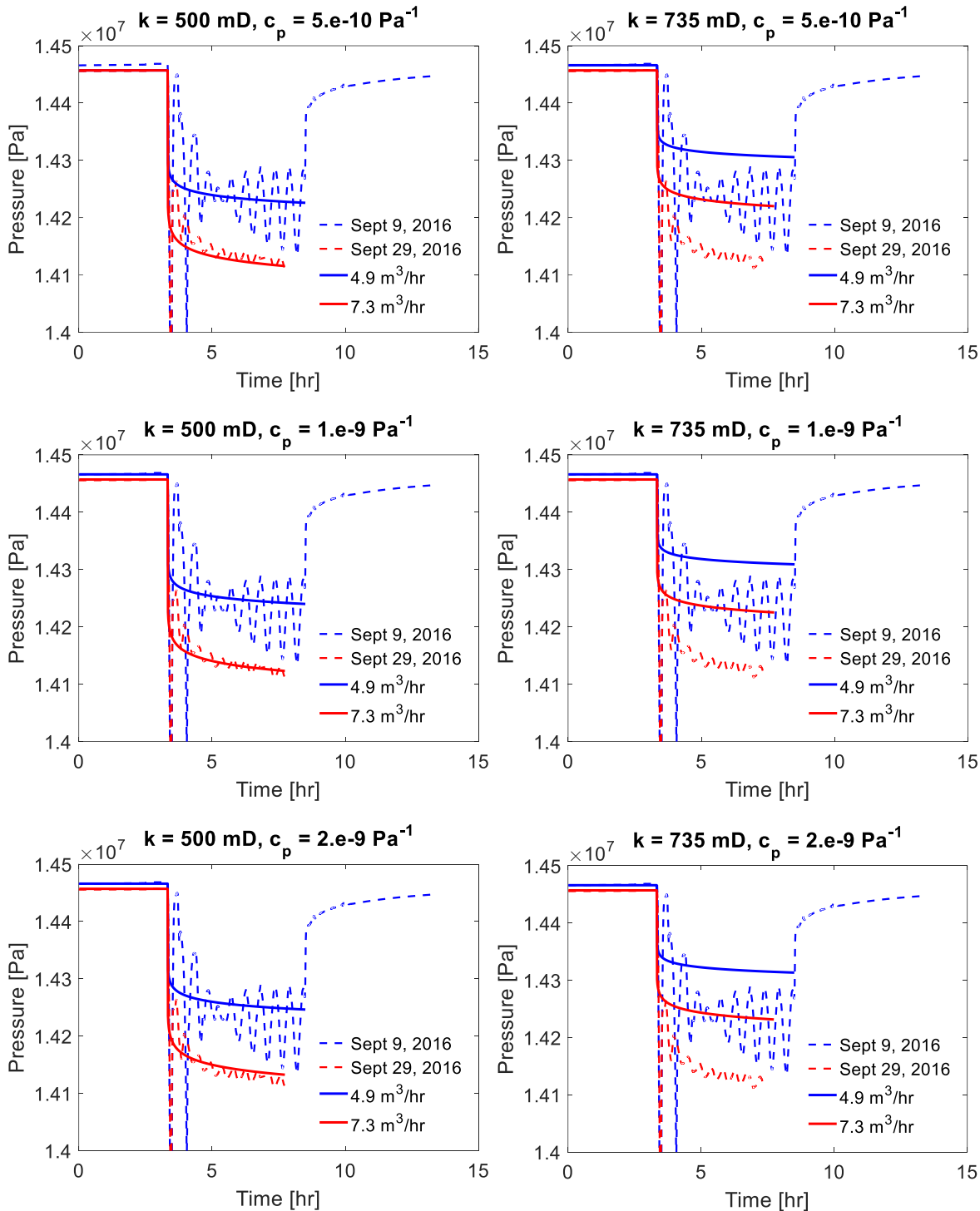


Figure 3. Comparison between hydraulic test data (see dash lines; both on September 9th and 29th) and the Theis solution (solid lines) for different parameter values of permeability and pore compressibility. Note that in each subplot, the same permeability is used for both tests, regardless of whether there is CO₂. The flow rates for both dates are averaged from pump readings.